Chinese Journal of Aeronautics, (2023), 36(6): 161–173

Chinese Society of Aeronautics and Astronautics
& Beihang University

Chinese Journal of Aeronautics

cja@buaa.edu.cn
www.sciencedirect.com

Downwash modelling for three-lifting-surface aircraft configuration design

Salvatore CORCIONE [a,*], **Giordana BONAVOLONTÀ** [b], **Agostino DE MARCO** [a], **Fabrizio NICOLOSI** [a]

[a] *Department of Industrial Engineering, University of Naples "Federico II", Naples 80125, Italy*
[b] *School of Aerospace Transport & Manufacturing, Cranfield University, Bedford MK43 0AL, United Kingdom*

Received 29 May 2022; revised 12 September 2022; accepted 18 September 2022
Available online 21 March 2023

KEYWORDS

Aerodynamic modelling;
Aircraft design;
Design of experiments;
Downwash;
Three-lifting-surface

Abstract This paper introduces a semi-empirical model to predict the downwash gradient at the horizontal tail of a three-lifting-surface aircraft. The superposition principle applied to well established formulations valid for two lifting surfaces is not a reasonable approach to calculate the downwash of a canard-wing-tail layout, and this paper demonstrates that such a basic technique leads to incorrect results. Therefore, an ad hoc prediction model is proposed that considers the combined nonlinear effects of canard and main wing inductions on tail downwash, being based on a full factorial design sweep of CFD simulations obtained by varying the main geometrical parameters of the three lifting surfaces. A suitable analytical formula for the downwash gradient is established through a process of data analysis and factor extraction. The presented model extends the validity of the available models for traditional two-lifting-surface designs by means of a correction factor. The engineering estimation method introduced here exhibits an acceptable accuracy, as well as relatively small prediction errors, and it is suitable for conceptual and preliminary studies of three-surface layouts. The value of this methodology is confirmed by the validation with the results of numerical and experimental investigations on a case study aircraft.

1. Introduction

In recent years, both market and environmental requirements have brought aircraft manufacturers and research institutes to explore and study alternative, non-conventional configurations for even more efficient transport aircraft. Two notable examples are the blended wing body[1,2], and the box wing[3–5] configurations. Another very promising alternative is the Three-Surface Aircraft (TSA) concept[7–10], which involves the integration of a third lifting surface, named "canard", ahead of a con-

* Corresponding author.
E-mail address: salvatore.corcione@unina.it (S. CORCIONE).
Peer review under responsibility of Editorial Committee of CJA.

ELSEVIER Production and hosting by Elsevier

https://doi.org/10.1016/j.cja.2023.03.035

ventional wing-tail arrangement. The engineering analysis of the aerodynamic interaction between the canard wake and the wing wake is not at all a trivial problem for the aircraft designer, especially because the three-surface layout selection strongly influences the design of each single component. Examples of well-known TSA designs are the Piaggio P180 Avanti (business turboprop), the Scaled Composite Triumph (demonstrator) and the Scaled Composite Catbird (general aviation).

Several studies on both the advantages and challenges of the TSA concept have been carried out during the last two decades.

The most important and recent research projects that involve optimization studies of TSA are the DLR internal project "Dreiflächen-Flugzeug (3FF)[11]", and the EU funded project IRON[12] (Innovative turbopROp configuratioN). In their early studies, Selberg and Rokhsaz[13] considered conventional wing-tail, canard-wing, and three-surface aircraft layouts to determine each configuration's induced as well as viscous drag under trimmed conditions. A three-surface vortex lattice method was used in that work to find aircraft trimmed flight conditions, and to predict the induced drag of each configuration.

Ostowari and Naik[14] performed a series of wind-tunnel experiments to investigate the aerodynamic characteristics for a three lifting-surface configuration. They produced some comparative data between the three-surface, canard, and conventional configurations, with identical fuselage, main wing, and vertical tail, in terms of lift curve slope, maximum lift coefficients, drag coefficient in cruise as well as at high lift condition, zero lift pitching moment coefficient and neutral point position. Patek and Smrcek[15] fulfilled a wind tunnel testing of a specially designed aircraft model allowing systematic variation of geometric parameters related to overall aircraft configurations. The aim was to provide basic aerodynamic data effects of multi-surface aircraft configurations with a view to assessing the degree to which specific design features such as a combination of canard, wing and tail plane are beneficial to aircraft aerodynamic performance. Nicolosi et al.[8] analysed different configurations for an innovative regional turboprop, including the TSA among them, and showed that a three-lifting-surface layout is a design solution that best complies with the challenging performance requirements for such a category of airplanes.

Another recent work carried out by the same authors confirms this feature because of a broader analysis of possible modern high-capacity turboprop aircraft designs and concludes that the TSA concept is potentially able to reduce the environmental impact of regional aircraft with respect to the current state-of-the-art regional jet widely adopted on short/medium hauls. The study presents three possible architectural solutions, as a starting point of a multi-disciplinary analysis and optimization process.

By comparing the results obtained for each optimum turboprop aircraft to a reference regional jet model, the Airbus A220-300 operated on a range of 1600 NM, Nicolosi et al.[16], demonstrate that a three-lifting-surface layout implies a maximum potential fuel saving of about 17%. This configuration allows a reduction of trim drag in cruise, providing a higher efficiency and higher maximum achievable lift coefficients.

In two successive studies, Corcione at al.[12,17] present the high-lift capabilities, as well as the longitudinal and directional aerodynamic characteristics of a three-lifting-surface aircraft resulting from several numerical simulations and wind tunnel tests. Significant effects due to the canard downwash and wake are highlighted in this work, especially in landing configuration with a canard deployed flap.[17] In clean conditions, instead, the most relevant canard effect is a significant reduction of the tail lift curve slope, of about 22% compared to the conventional two-surface layout. These two works demonstrate that the three-lifting-surface concept requires a careful design that should consider the whole canard-wing-tail arrangement, in particular the effect of canard on wing and tail aerodynamics as well as on the aircraft longitudinal stability.

Other studies are found in the literature on peculiar aspects of the TSA. For instance, Ruiz-Calavera et al.[18] analysed the aerodynamic properties of a three-lifting-surface configuration for an ultra-high-capacity airplane, showing that the arrangement of three coplanar surfaces, in an unstable configuration, seems to be the best compromise in terms of induced drag. In another study on a business/commuter advanced turboprop design, Owens and Perkins[19] presented their wind-tunnel tests on a three-surface configuration with a forward-swept wing. This research shows that a three-surface layout with aft-mounted engines can achieve a higher longitudinal stability, a reduced wing aerodynamic drag, and up to 20% increase in centre-of-gravity range with respect to conventional wing-tail designs.

Strohmeyer and Seubert at DLR[6] carried out sensitivity studies and canard optimizations on a three-lifting-surface aircraft by means of both numerical simulations and wind tunnel tests. Their analyses show that a swept back canard in low position with high aspect ratio, low taper ratio, and moderate span promises optimum performance in terms of fuel savings.

The amount of research and accumulated investigations over the years on the subject suggest that a three-lifting-surface configuration provides the following advantages over the conventional wing-tail design: more flexibility in selecting the aircraft geometry in terms of payload-wing-fuselage relative positions, compliance with control and stability requirements over an extended centre of gravity range under all certified flight conditions, reduction of trim drag over a wide centre of gravity range, load reduction on the main wing, reduction of the total lifting area required to fly with consequent reduction of the total wetted area and drag, increment of the whole aircraft maximum lift capabilities, safe wing stall behaviour, reduction of the horizontal tail plane load to trim the aircraft in cruise, shorter take-off and landing paths, larger payload at fixed wing size.[6]

However, a TSA also comes with disadvantages like additional parasite drag, higher weight, decrease of both longitudinal and directional stability, especially in high-lift conditions if a canard flap is deployed, quite different aeroelastic characteristics with respect to conventional designs.[6]

This research effort focuses on the downwash generated by the combination of both canard and wing at the tail: this phenomenon deserves a special consideration in designing a TSA since it affects the aerodynamic characteristics of the tail plane in such a way it may become a key driver in sizing it. In particular, a reliable estimation of the tail downwash gradient for a canard-wing-tail arrangement is required since the early stages of the design process.

The literature offers several methods to predict the downwash behind the main wing for a conventional two-lifting-surface aircraft configuration. These include both linear and non-linear approaches, like Roskam,[20] Silverstein and

Katzoff,[21,22] Finck[23] (DATCOM), or Slingerland.[24] In general, these methods estimate the influence of the main lifting surface on the aft tail by calculating the downwash gradient in the symmetry plane at the longitudinal and vertical position of the tail reference point. Then, a correction factor can be applied to account for the downwash angle spanwise variation. The latter can be discarded in a conventional wing-tail combination, being the tail span usually much smaller than the wingspan.

Conversely, in the case of either a canard or a TSA configuration the downwash spanwise variation at both the wing and the tail becomes quite significant since the canard span is smaller than the wingspan and is comparable to the tail span. A first attempt to provide a prediction method for the downwash gradient at the wing in presence of a canard has been proposed by Philips[25,26]. In these works, a closed-form solution for the downwash at the symmetry plane of an elliptically loaded wing is theoretically derived and then the average downwash gradient is calculated. However, this method does not account for the actual wing geometry and is valid for an ideal wing loading distribution, hence it provides no practical design indications.

The effect of a canard surface on the total lift of an unswept wing in subsonic flow was studied by Rasmussen[27], who calculated the downwash on the wing by replacing the canard with a single horseshoe vortex. The work introduces an application of the aerodynamic reciprocity theory, which is rather complex and valid only under certain assumptions, i.e., symmetrical unswept wing, elliptic lift distribution, wing that lies directly in the wake of the canard.

Another method to predict the induction caused by a canard has been proposed by Levy[28], who uses a simple methodology based on a vortex lattice approach to calculate the downwash in the wing symmetry plane as well as the spanwise attenuation factor. This method is valid only when both wing and canard have the same aspect ratio. As in the case of both Roskam[20] and Rasmussen[27] methods, also the approach proposed by Levy[28] is provided via charts.

Yet, regarding the case of a three-lifting-surface layout, no well documented methods are found in literature that estimate the tail downwash gradient generated by the interaction of both canard and wing. The present work introduces a semi-empirical method to quickly predict the gradient of the mean tail downwash with respect to the angle of attack in a canard-wing-tail combination. The formulation is set in such a form that the desired gradient is obtained after multiplying the tail downwash gradient of the wing-tail pair by a properly derived correction factor accounting for the presence of a third lifting surface ahead of the main wing. By providing a correction factor, the proposed method relies on the validity of well assessed methods that predict the downwash gradient at the tail plane of a conventional wing-tail arrangement and extends their applicability to a TSA configurations.

This paper is organized as follows. Section 2 introduces the problem statement and demonstrates that the superposition principle is not a valid approach to solve it. Section 3 describes the methodology and the tools used to formulate the semi-empirical estimation method. Successively, Section 4 presents the method, obtained in terms of an analytical formula and a set of regression coefficients, and quantifies the errors. In addition, a test case is presented to validate the approach. Finally, in Section 5 conclusions are drawn and future work steps are highlighted.

2. Materials and methods

2.1. Problem statement

The Computer Aided Design (CAD) representation of a possible three-lifting-surface arrangement is shown in Fig. 1.[29] This representation defines α as the angle of attack of the free stream velocity vector with respect to the wing root chord, and the local angle of downwash $\tilde{\varepsilon}_{\mathrm{H(CW)}}|_{y_H=0}$ at the tail symmetry plane. According to the common definition, the downwash $\varepsilon_{\mathrm{H(CW)}}$ is the mean value over the tail span of the local sectional deviation angle $\tilde{\varepsilon}_{\mathrm{H(CW)}}(\eta_{\mathrm{H}})$, as a function of the spanwise nondimensional coordinate $\eta_{\mathrm{H}} = 2y_{\mathrm{H}}/b_{\mathrm{H}}$. A schematic of the three-lifting-surface layout is depicted in Fig. 2, where the main relative positioning parameters are indicated. This work addresses the problem of finding a convenient prediction model of the downwash gradient $\mathrm{d}\varepsilon_{\mathrm{(CW)}}/\mathrm{d}\alpha$ for an aerodynamic configuration so defined.

In such a configuration, the total downwash at the horizontal tail is significantly influenced by the presence of a canard. This can be readily seen in Fig. 3,[30] which displays some selected streamlines passing near the tail for different angles of attack. These streamlines are traced from the same set of points in the flow field and serve to compare two scenarios: (A) a conventional wing-tail configuration, and (B) the same wing-tail arrangement augmented by adding a canard surface ahead of the wing. When both perspective views and side views are compared, the effect of a canard is evident in terms of streamline deviation due to the induced downwash at the tail. This is even more clear when projecting the velocity field in a vertical reference plane placed slightly ahead of the tail, normal to the configuration symmetry plane (see the dashed lines in the side views of Fig. 3). In such a plane the induced deviation angle of the airflow is calculated as the inverse tangent of V_z/V_∞ where V_z is the vertical component of the local flow velocity vector. The induced angle of deviation is shown in Fig. 4.[30] for both scenarios. The presence of a lifting surface ahead of the wing determines higher downward ($V_z < 0$) deviation angles, due mainly to the pair of counter-rotating vortices shed by the two canard tips.

A first approach to account for the effect of both canard and wing is to calculate the total downwash gradient at the tail by applying the superposition principle, that is, by simply summing up the contributions to the desired downwash gradient

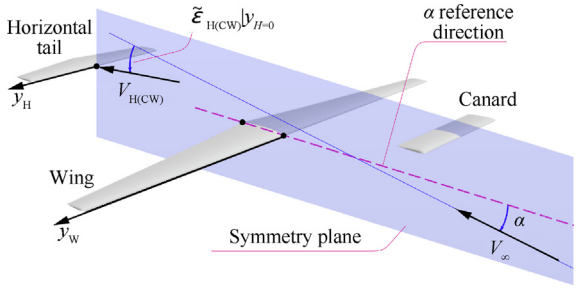

Fig. 1 CAD geometry of a three-lifting surface configuration, automatically generated by the JPADCAD geometry processing tool[29]. Definitions of angle of attack and of local downwash angle at tail symmetry plane.

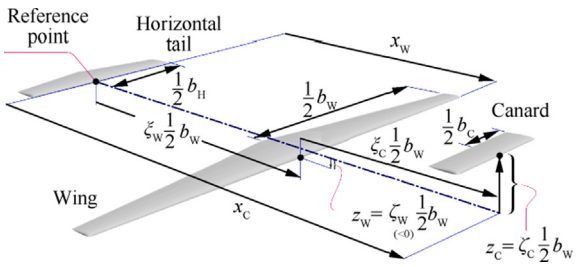

Fig. 2 Positioning parameters of wing and canard with respect to a reference point at the leading edge of tail root chord. Distances x_W and x_C positive rear to front (with $x_W < x_C$), z_W and z_C positive bottom to top.

$d\varepsilon_{H(CW)}/d\alpha$ due to canard only and to wing only, respectively. Such a technique brings the advantage that a downwash gradient estimation is easily obtainable with well-known low-fidelity methods available in literature and developed for two-lifting-surface configurations. Yet the superposition method is certainly approximate, even within the range of angles of attack where the total lift coefficient is linear with α. This is demonstrated by the comparative results of selected calculation examples reported in Table 1.

The comparison considers three layouts: a representative canard-wing-tail arrangement, and two related configurations obtained by leaving out the canard and the wing, respectively. These geometries have been analysed with CFD simulations at different angles of attack and in all cases the tail lift coefficient slope has been calculated: $C_{L_{\alpha,H(CW)}}$ (tail in presence of both canard and wing), $C_{L_{\alpha,H(W)}}$ (tail in presence of wing only), $C_{L_{\alpha,H(C)}}$ (tail in presence of canard only).

The tail lift coefficient slopes have been used to calculate the mean tail downwash gradients according to the method proposed by Barlow et al.,[31] which has been extensively used to evaluate downwash gradients from wind tunnel data.

For instance, in case of a simple wing-tail combination, one can assume that the tail lift coefficient is given by

$$C_{L_{H(W)}} = C_{L_{\alpha,H}}\left(\alpha - \alpha_{0L_H} + i_H - \varepsilon_{H(W)}\right) \tag{1}$$

where $C_{L_{\alpha,H}}$ is the known value of the isolated tail lift curve slope. By derivation of Eq. (1) with respect to α, the tail lift curve slope in presence of a wing only is expressed as follows:

$$\frac{\partial C_{L_{H(W)}}}{\partial \alpha} \equiv C_{L_{\alpha,H}} - C_{L_{\alpha,H}}\frac{d\varepsilon_{H(W)}}{d\alpha} \tag{2}$$

and finally, the downwash gradient takes the following form:

$$\frac{d\varepsilon_{H(W)}}{d\alpha} = \frac{C_{L_{\alpha,H}} - C_{L_{\alpha,H(W)}}}{C_{L_{\alpha,H}}} = 1 - \frac{C_{L_{\alpha,H(W)}}}{C_{L_{\alpha,H}}} \tag{3}$$

Similar expressions are readily obtained for the gradients $d\varepsilon_{H(C)}/d\alpha$, and $d\varepsilon_{H(CW)}/d\alpha$, that is

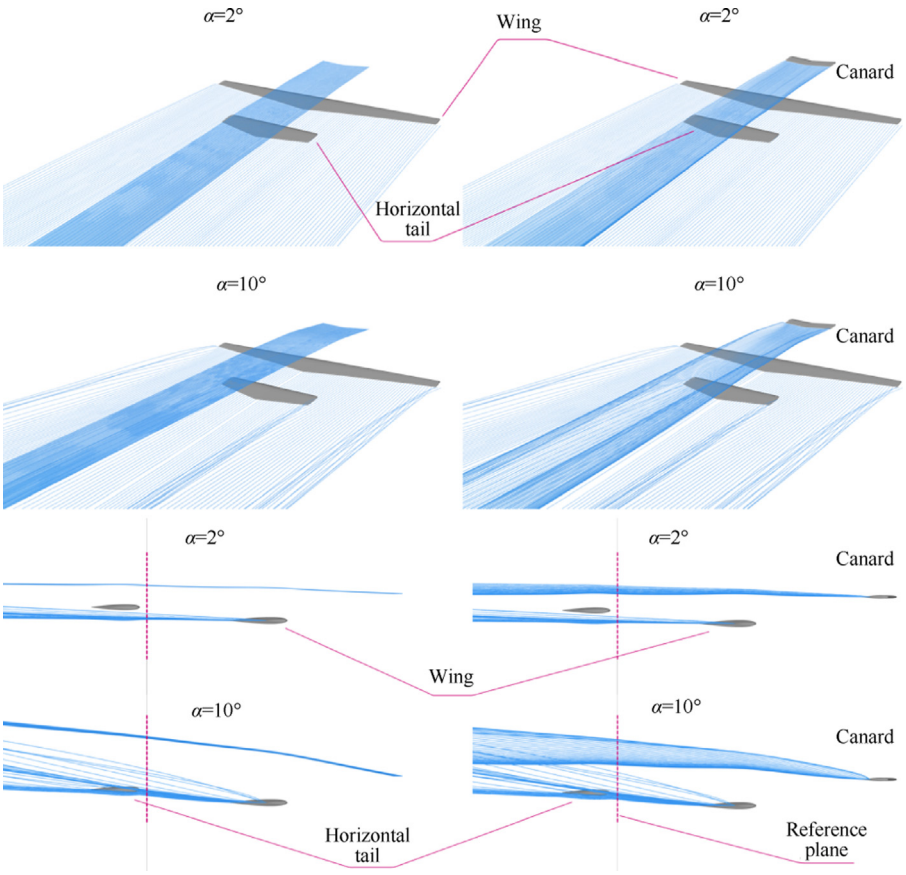

Fig. 3 Streamlines over a tail in presence of wing only (left) and in presence of both canard and wing (right). Layout parameters: $\xi_C = 0.5$, $\zeta_C = 0.06$, $\xi_W = 0.6$, $\zeta_W = -0.06$. Results obtained from CFD simulations in Simcenter STAR-CCM+software.[30]

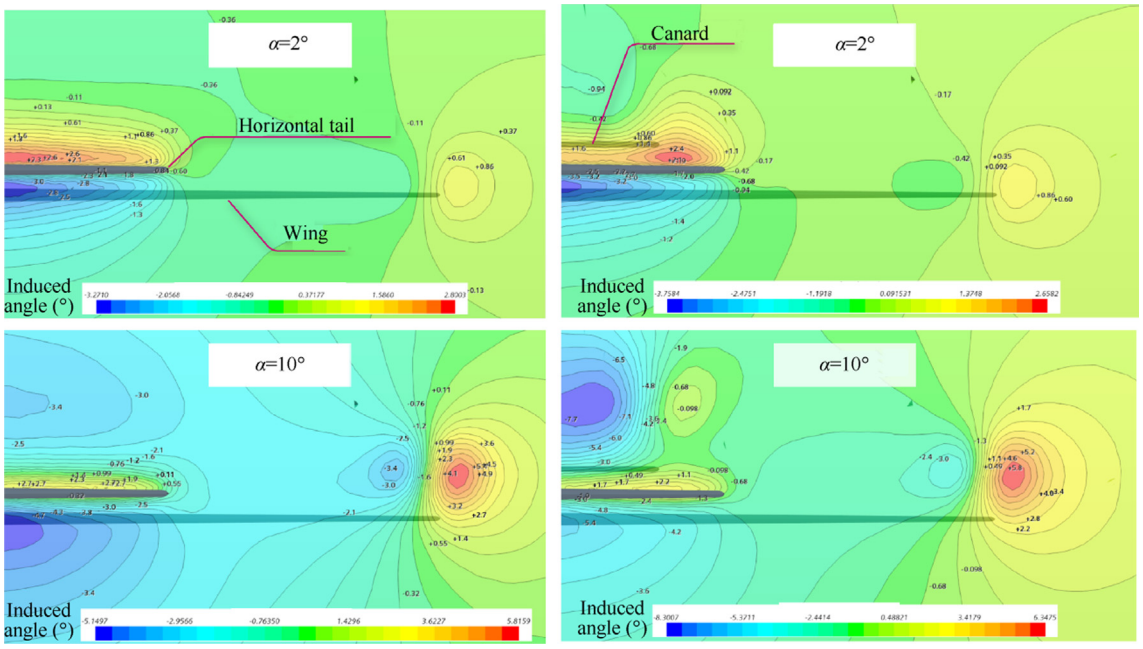

Fig. 4 Induced angle of flow deviation from free stream velocity direction in a plane slightly ahead of horizontal tail (see reference plane in Fig. 3), in presence of wing only (left), and in presence of both canard and wing (right). Layout parameters: $\xi_C = 0.5$, $\zeta_C = 0.06$, $\xi_W = 0.6$, $\zeta_W = -0.06$. Results obtained from CFD simulations in Simcenter STAR-CCM + software.[30]

Table 1 Percentage error given by superposition approach to calculate downwash gradient at the tail of a three-lifting-surface configuration (case of $\xi_C = 0.5$, $\zeta_C = 0$, $\xi_W = 0$).

Canard-horizontal tail	Wing-horizontal tail		Canard-wing-horizontal tail	
$d\varepsilon_{H(C)}/d\alpha$	$d\varepsilon_{H(W)}/d\alpha$		$d\varepsilon_{H(CW)}/d\alpha$	Error (%)
CFD	CFD	CFD	$d\varepsilon_{H(C)}/d\alpha + d\varepsilon_{H(W)}/d\alpha$	
0.15	0.33	0.39	0.48	23

$$\begin{cases} \frac{d\varepsilon_{H(C)}}{d\alpha} = 1 - \frac{C_{L_{\alpha,H(C)}}}{C_{L_{\alpha,H}}} \\ \frac{d\varepsilon_{H(CW)}}{d\alpha} = 1 - \frac{C_{L_{\alpha,H(CW)}}}{C_{L_{\alpha,H}}} \end{cases} \tag{4}$$

The ratios in the above formulas can be determined from numerical (see Fig. 5) or wind tunnel experiments and include both the effects of tail dynamic pressure ratios $\bar{q}_{H(.)}/\bar{q}_\infty$ and of the downwash itself.

Results of Table 1 clearly show that the estimate of $d\varepsilon_{H(CW)}/d\alpha$ provided by the superposition approach is affected by a significant error when compared to the CFD simulated output. Hence, this work introduces a specific estimation method for the mean downwash gradient at the tail of a TSA, given by the following formula:

$$\frac{d\varepsilon_{H(WC)}}{d\alpha} = k_C \frac{d\varepsilon_{H(W)}}{d\alpha} \tag{5}$$

The proposed model provides the correction factor k_C as a suitable function of the canard-wing-tail combination geometric parameters, that simply adjusts the downwash gradient $d\varepsilon_{H(W)}$ of a conventional wing-tail pair. The latter is obtainable with any of the calculation methods already available in literature. With this technique the desired gradient $d\varepsilon_{H(CW)}$, of the same configuration but augmented with a canard surface, will be readily predicted. The following section discusses the methodology adopted to establish a dependence of k_C on a proper set of the configuration parameters.

2.2. Methodology and tools

Different tools and procedures are necessary to develop a method able to define the correction factor k_C as a suitable function of the configuration geometry. As a first step, a sensitivity analysis on the main canard design parameters is required to identify those that significantly affect the downwash gradient at the tail.

For this purpose, the fluid flow over several three-lifting-surface layouts has been analysed, keeping in all cases a fixed planform of both wing and tail, with fixed x_W and z_W, i.e., $\xi_W = 2x_W/b_W = 0.6$, and $\zeta_W = 2z_W/b_W = -0.06$. The approach of initially keeping a frozen wing-tail pair is suggested by the chosen model defined by Eq. (5).

The reference wing-tail baseline combination has been taken from the work of Nicolosi et al.[12] who investigated the

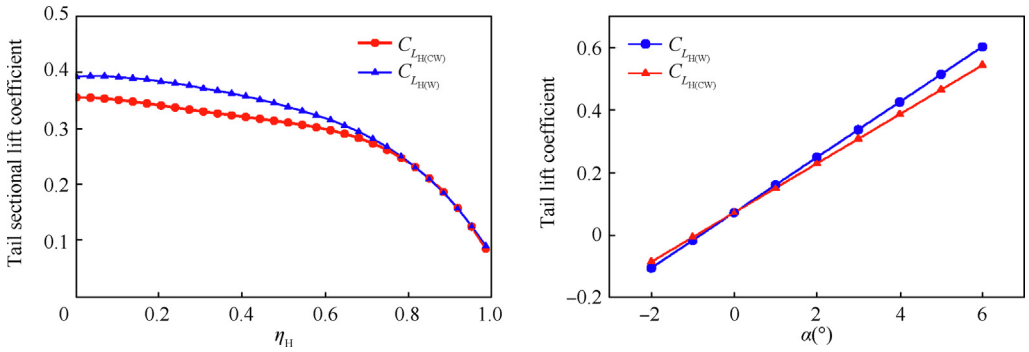

Fig. 5 (Left) Tail sectional lift coefficient versus nondimensional coordinate $\eta_H = 2y_H/b_H$, in presence of wing only, and in presence of both canard and wing $C_{L_{H(CW)}}$ at the same wing angle of attack = 2°. (Right) Tail lift coefficients at different angles of attack. Results obtained from CFD simulations in STAR-CCM+[30] on a fixed layout, $\xi_C = 0.5$, $\zeta_C = 0$, $\xi_W = 0.6$, $\zeta_W = 0$.

three-lifting surface concept for innovative large turboprop airplanes. For the sake of simplicity, an untwisted NACA-0012 airfoil has been selected as a unique sectional shape to all lifting surfaces considered in this study, assuming that the problem is not dominated by parameters like twist or airfoil curvatures and thicknesses. This assumption is supported by the fact that the target of this study is the estimate of the canard and main wing inductions on tail downwash gradient, that will be evaluated by comparing the lift curve slope of lifting surfaces in the linear range of angles of attack.

Regarding the canard position within the three-surface layout, the main design variables are: the nondimensional horizontal $\xi_C = 2(x_C - x_W)/b_W$ and vertical $\zeta_C = z_C/b_W$ relative positions between canard and tail, the canard-tail span ratio (b_C / b_H), the canard sweep angle (Λ_C), and the canard taper ratio (λ_C). This set of parameters has been used to generate a full factorial experiment,[32] whose discrete values are reported in Table 2. The ranges have been chosen according to the typical dimensions of existing transport aircraft. For the variables ζ_C and Λ_C, both negative and positive values have been considered.

The full factorial design (also called "five-factor design", or $2 \times 3 \times 2 \times 3 \times 2 = 72$) has been carried out by means of numerical simulations. Since this work focuses on how the canard affects the total downwash gradient at the tail, at low incidence and low Mach number, the choice of a convenient technique to simulate the flow could have fallen on a low fidelity numerical approach, e.g., a Vortex Lattice Method (VLM) or a panel method. This was the choice of Levy[28] and Jansen.[33]

Low fidelity aerodynamic solvers are, in fact, widely used for conceptual and preliminary studies, mainly for their low computational cost. Yet some limitations and issues arise when they are applied to configurations with more than two lifting surfaces, where the wakes in some common cases may strongly interact and give poor results.

For this reason, in the present effort all three-surface combinations in the full factorial design have been simulated with a high fidelity inviscid CFD simulations using Siemens' Simcenter STAR-CCM+.[30] All CAD geometries and volumetric grids were automatically generated by coupling the JPADCAD geometry processing tool with STAR-CCM + automation features as discussed by de Marco et al.[29]

Regarding the simulation set-up, Fig. 6 shows a full view of the typical fluid domain and how the boundary conditions are imposed, while Table 3 summarizes the fluid domain size and the polyhedral mesh settings. Some close-up views of a polyhedral mesh are displayed in Fig. 7 and Fig. 8 showing the quality of the grids in the full factorial design. The refinements were generated automatically in STAR-CCM + with a set of local customized surface controls on the leading edge and on rounded tips of each lifting surface. All simulations have been performed in air at sea level conditions, for a free stream Mach number of 0.2. Since the key objective is the lift curve slope of the tail plane with and without the presence of the third lifting surface ahead of the main wing, simulations have been performed only for two angles of attack in the linear range of the lift coefficient (0° and 4°). To ensure the simulation results are independent of the underlying mesh, a parametric investigation has been performed targeting the convergence of the tail

Table 2 Selected values of nondimensional design variables.

Parameter	Value
$\xi_C = 2(x_C - x_W)/b_W$	{0.5,2}
$\varsigma_C = 2z_C/b_W$	{-0.3,0,0.3}
b_C/b_H	{0.6,1.1}
$\Lambda_C(°)$	{-30,0,30}
λ_C	{0.4,1}

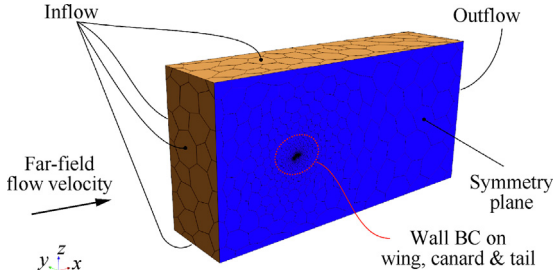

Fig. 6 Fluid domain and boundary conditions. Computational domain and volumetric grid automatically generated by the JPADCAD geometry processing tool[29] using STAR-CCM+[30] automation features.

Table 3 General mesh settings and custom controls settings in STAR-CCM + for all lifting surfaces. Typical mesh dimensions per single case.

Pamameter		Value
Domain size	Block span (m)	345 (~20 b_W/2)
	Block height (m)	345 (~20 b_W /2)
	Block length	1380 (~80 b_W /2)
General mesh settings	Base size (m)	{150, 100, 90, 80}
	Cells	{835577, 1763838, 2235469}
	Target surface size (%)[b]	100
	Surface grow rate	1.1
Custom controls[a]	Target surface size (%)[b]	0.2
	Minimum surface size (%)[b]	0.005
Final polyhedral mesh statistics	Base size (m)	100
	Cells	1763838
	Faces	12682394
	Vertices	110301372

Note: superscript a and b represent for all lifting surfaces and percentage of base size.

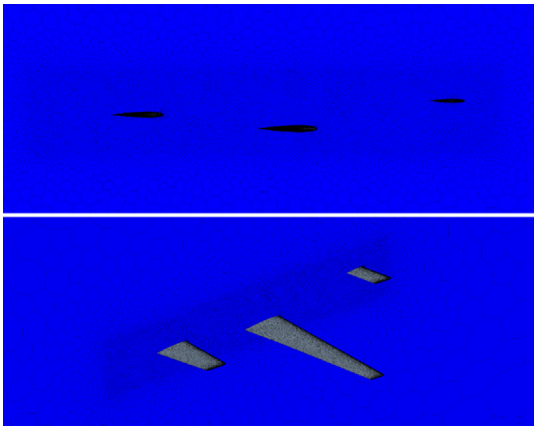

Fig. 7 Close up view of polyhedral mesh at symmetry plane and on three lifting surfaces. CAD geometries and volumetric grid automatically generated with the JPADCAD processing tool[29] coupled to STAR-CCM + [30] automation features.

lift slope in the canard, wing and tail arrangement of the validation case configuration introduced in Section 4. Since all mesh parameters have been defined as a percentage of a reference length, the parametric study has been fulfilled by changing the base size parameter. Table 3 reports the different values used for the base size and the corresponding number of mesh cells as well as the characteristics of the selected final mesh.

Fig. 9 shows how the number of mesh cells impacts the prediction of the horizontal tail lift curve slope evaluated in the linear range of angle of attack between 0° and 4°. The chart clearly shows that the trend becomes constant from the 1.7 million cells mesh. Thus, to reduce the computational burden of the parametric study discussed in the next section, a base size of 100 m has been selected without any accuracy loss.

Two convergence criteria have been imposed: (A) the highest residual value must not exceed 10^{-4} and (B) the maximum difference between 500 tail lift coefficient samples (normalized with the mean value) must be lower than 10^{-5}. A maximum number of iterations has been imposed to 5000 in case the convergence criteria are not satisfied. Fig. 10 shows the case convergence for two angles of attack: 0° and 4°. Residuals and lift coefficient of the horizontal tailplane are plotted against the number of iterations, as it can been seen the convergence criteria are satisfied within 1000 iterations per angle of attack.

An n-way ANOVA (Analysis Of Variance)[32] has been conducted using MATLAB Statistics and Machine Learning Toolbox[34] on the full factorial design results. Analysis of variance is a statistic analysis tool able to find out which are the systematic factors and the random factors inside a dataset. The systematic factors do have a statistical influence on the aggregated variability of the dataset, while the random factors do not. This, applied in a regression study, allows to determine the independent variables which statistically affect the variability of the dependent variable the most.

In this study, the calculated ratio (correction factor):

$$k_C = \frac{d\varepsilon_{H(CW)}}{d\alpha} \Big/ \frac{d\varepsilon_{H(W)}}{d\alpha} \tag{6}$$

has been used as a dependent variable, while the independent variables are the one already presented in Table 2. The terms $d\varepsilon_{H(WC)}/d\alpha$ and $d\varepsilon_{H(C)}/d\alpha$ at the right-hand-side of Eq. (6) have been calculated from numerical solutions according to Eqs. (3) and (4). Successively, the number of levels of each parameter has been increased within the ranges previously defined, and

Fig. 8 Close up views of refined surface mesh: (Left) canard tip and (Right) wing leading edge at intersection with the symmetry plane. Rounded tips and surface grid refinement automatically generated with the JPADCAD geometry processing tool[29] coupled to STAR-CCM + [30] automation features.

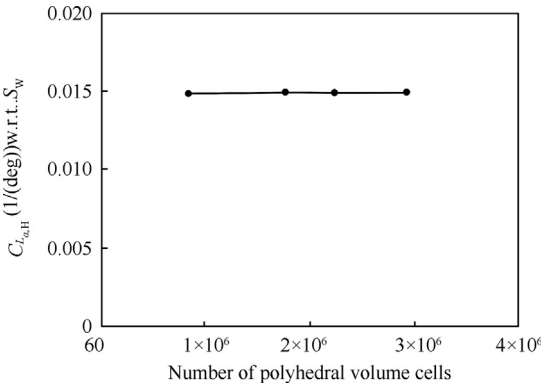

Fig. 9 Mesh independence analysis: lift curve slope of horizontal tailplane versus the number of volume cells. The investigated configuration is the wing-canard-tail arrangement of the validation case presented in Section 4. Results obtained from CFD simulations in Simcenter STAR-CCM + software.[30]

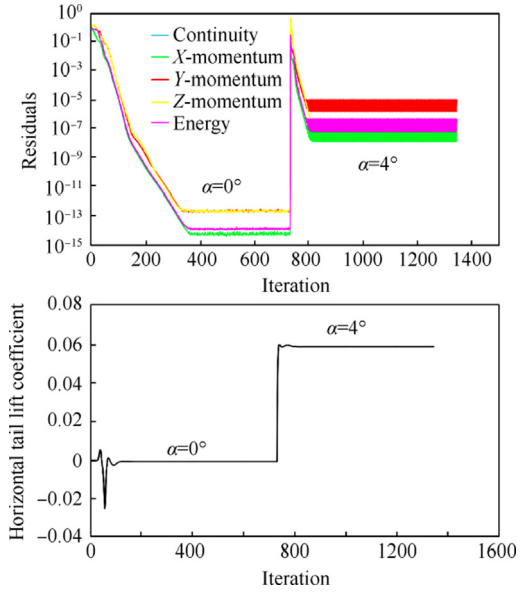

Fig. 10 Case convergence for two angles of attack: residuals and horizontal tailplane lift coefficient versus the iterations number. Investigated configuration is the validation case shown in Section 4. Results obtained from CFD simulations in Simcenter STAR-CCM + software.[30]

an analytical estimation method for k_C has been extracted in terms of a multivariate polynomial expression. The details of this process are discussed in next section.

3. Results and discussion

In this section the results of the whole analysis process are presented and discussed. The outcome of the ANOVA is shown in Table 4, where the significant set of canard parameters turns out to be the following: $\{\xi_C, \zeta_C, b_C/b_H\}$. They have in fact a p-value that is smaller than a significance level of 0.05 (see Montgomery[35]).

This means that for each of the three geometrical parameters there is less than 5% probability that the variable is not useful in predicting the downwash correction factor.

In the present study, the interaction or dependence between variables, i.e., the possibility that the impact of one factor on the response variable can depend on the level of one other factor, has been neglected, since retained of a minor importance in a preliminary screening study. Additionally, it is conceivable that strong interaction effects are present in non-linear aerodynamic conditions that are out of the scope of this work.

As a further analysis step, a second ANOVA has been conducted on the same data set but excluding all the non-significant parameters, to ensure the effectiveness of the remaining ones. The results of this second ANOVA, shown in Table 5, highlight that a variation of the longitudinal canard distance ξ_C from the tail, that is, for a fixed wing-tail combination, the canard distance $\xi_C b_W/2$ from the wing, does not involve a variation of tail downwash gradient.

Having identified the significant variables, the data set has been extended as follows: two extra levels of ξ_C, for a total of five levels (−0.3, −0.2, 0, 0.2, and 0.3), and two extra levels of the canard-tail span ratio, for a total of four levels b_C/b_H (0.6, 0.7, 0.9, and 1.1), have been added, and all the combinations among them have been analysed to generate the model. At this point, the constraint on the fixed wing-tail vertical offset has been relaxed by introducing a set of three different values of ζ_W (−0.2, 0, and 0.2) and all the inherent three-surface layouts have been simulated.

Moreover, each configuration has been also analysed for two different values of ξ_C: although this variable was qualified as not significant, its minor effect has been included on average to improve the accuracy of the model. Overall, the final predicting formula for k_C has been built based on 120 simulation cases.

Fig. 11 shows the simulated values of k_C collected as a function of ξ_W, ζ_C and b_C/b_H. The plots suggest that k_C linearly increases with the span ratio, for each fixed value of ζ_C and ζ_W. This is well expressed by the following linear regression formula:

$$k_C\left(\varsigma_C, \varsigma_W, \frac{b_C}{b_H}\right) = a(\varsigma_C, \varsigma_W)\frac{b_C}{b_H} + b(\varsigma_C, \varsigma_W) \tag{7}$$

where both the slope a and the intercept b depend on the other two variables involved, i.e. the canard-tail and the wing-tail vertical offsets.

Fig. 12 reports the quantities a and b obtained from linear regressions of Fig. 11 against ζ_C for each of the three simulated values of ζ_W, suggesting that they both exhibit a cubic trend in terms of canard vertical position. This behaviour is well represented by the following polynomial models for a and b:

$$\begin{cases} a_i(\varsigma_W) = a_0(\varsigma_W) + a_1(\varsigma_W)\varsigma_C + a_2(\varsigma_W)\varsigma_C^2 + a_3(\varsigma_W)\varsigma_C^3 \\ b_i(\varsigma_W) = b_0(\varsigma_W) + b_1(\varsigma_W)\varsigma_C + b_2(\varsigma_W)\varsigma_C^2 + b_3(\varsigma_W)\varsigma_C^3 \end{cases} \tag{8}$$

A last regression was made upon the different coefficients of the above polynomials, to obtain the fitting functions $a_i(\zeta_W)$ and $b_i(\zeta_W)$, for $i = 0,1,2,3$.

Fig. 13 and Fig. 14 show these functions against the wing vertical position: in this case three values of ζ_W were used, and the following parabolic expressions are a good fit for the data:

Table 4 Results of the first ANOVA on initial data set.

Parameter	Sum of squares	Degree of freedom	Mean squares	*F*-statistic	*p*-value
ξ_C	0.00169	1	0.00169	7.64	0.0074
ζ_C	0.03177	2	0.01589	71.87	0
b_C/b_H	0.02735	1	0.02735	123.73	0
Λ	0.00051	2	0.00025	1.15	0.3245
λ	0.00006	1	0.00006	0.26	0.6112
Error	0.01415	64	0.00022		
Total	0.07553				

Table 5 Results of the second ANOVA on the initial data set.

Parameter	Sum of squares	Degree of freedom	Mean squares	*F*-statistic	*p*-value
ξ_C	0.00028	1	0.00028	0.94	0.3653
ζ_C	0.00530	2	0.00265	7.81	0.0123
b_C/b_H	0.00456	1	0.00456	15.17	0.0059
Error	0.00210	7	0.00030		
Total	0.01224				

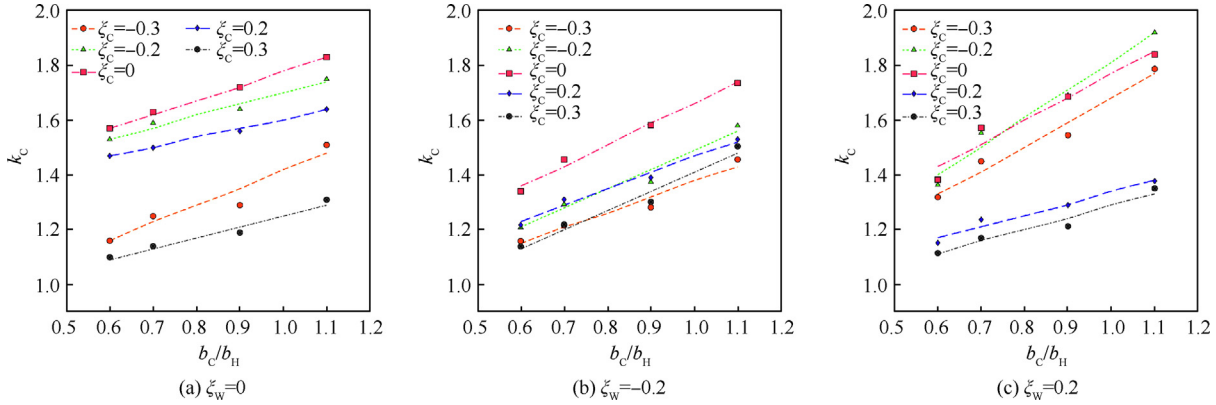

Fig. 11 Correction factor as a function of canard-tail span ratio b_C/b_H for different values of ζ_W.

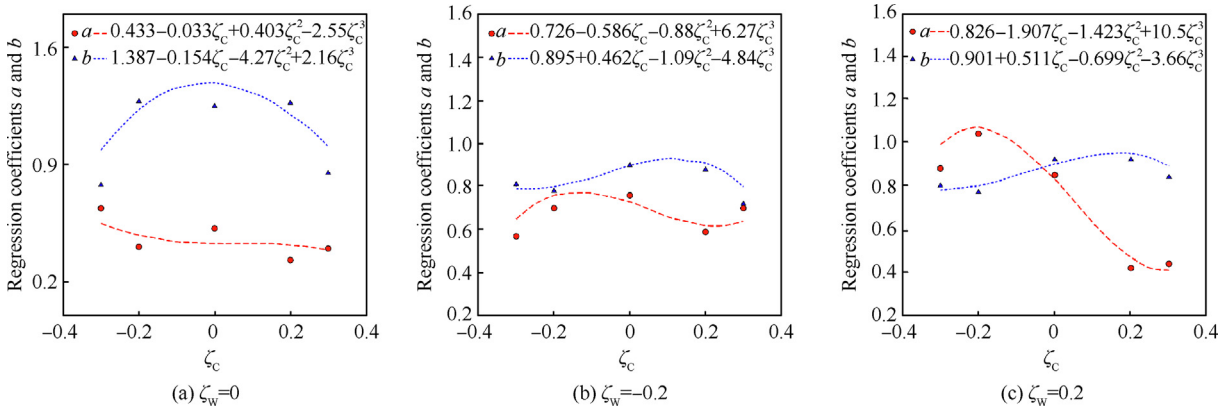

Fig. 12 Regression coefficients a (red) and b (blue) for three values of ζ_W.

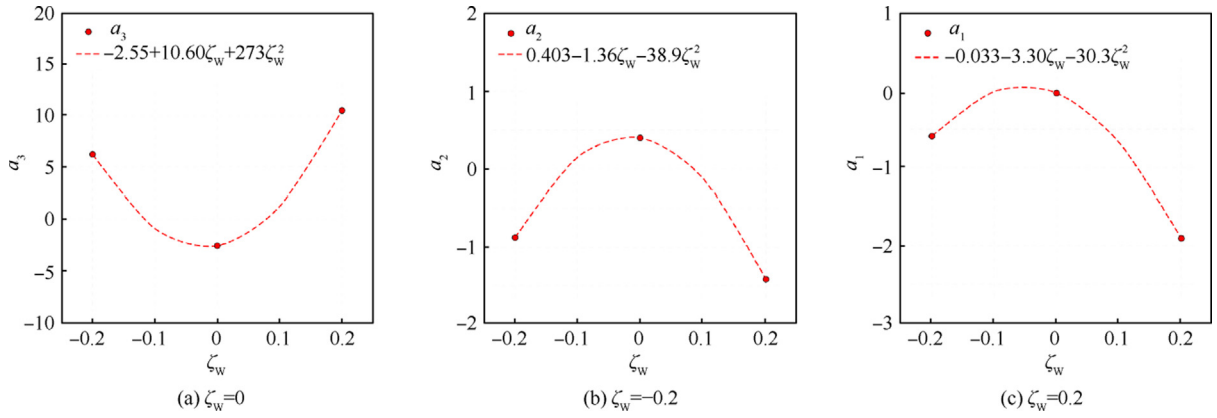

Fig. 13 Regression coefficients a_3, a_2, a_1, a_0 as a function of ζ_W.

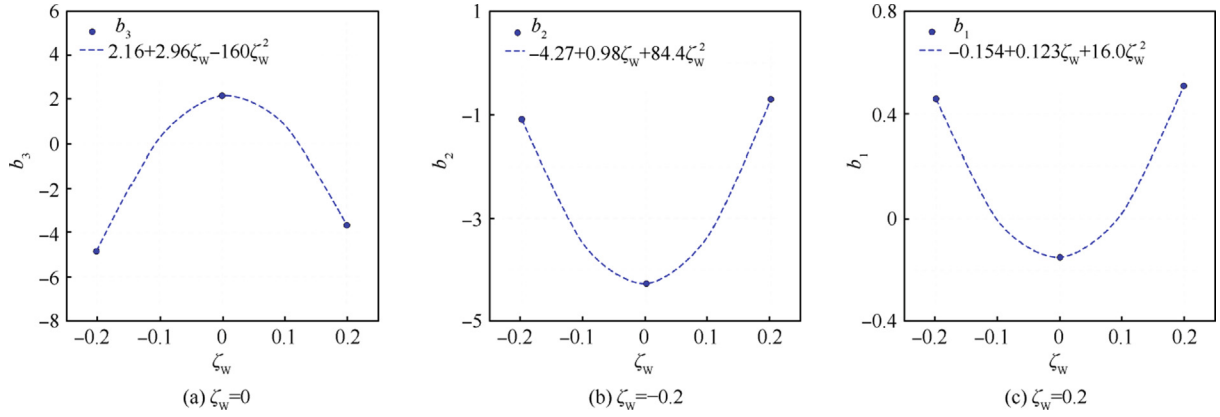

Fig. 14 Regression coefficients b_3, b_2, b_1, b_0 as a function of ζ_W.

$$\begin{cases} a_i(\varsigma_W) = a_{i0} + a_{ii}\varsigma_W + a_{i2}\varsigma_W + a_3\varsigma_W^2 \\ b_i(\varsigma_W) = b_{i0} + b_{i1}\varsigma_W + b_{i2}\varsigma_W + b_3\varsigma_W^2 \end{cases} i = 0,1,2,3 \tag{9}$$

There are 24 regression coefficients involved in the above two formulas, which are reported in Table 6. The final formulation that predicts k_C as the downwash correction factor to account for the presence of a canard in a three-lifting surface configuration is obtained by combining Eqs. (7)–(9) and takes the following form:

$$\begin{aligned} k_C\left(\varsigma_C,\varsigma_W,\tfrac{b_C}{b_H}\right) &= \left[(a_{00} + a_{01}\varsigma_W + a_{02}\varsigma_W^2) + (a_{10} + a_{11}\varsigma_W + a_{12}\varsigma_W^2)\varsigma_C\right. \\ &\left.+(a_{20} + a_{21}\varsigma_W + a_{22}\varsigma_W^2)\varsigma_C^2 + (a_{30} + a_{31}\varsigma_W + a_{32}\varsigma_W^2)\varsigma_C^3\right]\tfrac{b_C}{b_H} \\ &+\left[(b_{00} + b_{01}\varsigma_W + b_{02}\varsigma_W^2) + (b_{10} + b_{11}\varsigma_W + b_{12}\varsigma_W^2)\varsigma_C\right. \\ &\left.+(b_{20} + b_{21}\varsigma_W + b_{22}\varsigma_W^2)\varsigma_C^2 + (b_{30} + b_{31}\varsigma_W + b_{32}\varsigma_W^2)\varsigma_C^3\right] \end{aligned} \tag{10}$$

The function defined by Eq. (10) can be also arranged in matrix form as follows:

$$\begin{aligned} k_C\left(\varsigma_C,\varsigma_W,\tfrac{b_C}{b_H}\right) &= \begin{bmatrix}1 & \varsigma_C & \varsigma_C^2 & \varsigma_C^3\end{bmatrix}\left(\begin{bmatrix} a_{00} & a_{01} & a_{02} \\ a_{10} & a_{11} & a_{12} \\ a_{20} & a_{21} & a_{22} \\ a_{30} & a_{31} & a_{32}\end{bmatrix}\begin{bmatrix}1 \\ \varsigma_W \\ \varsigma_W^2\end{bmatrix}\right)\tfrac{b_C}{b_H} \\ &+\begin{bmatrix}1 & \varsigma_C & \varsigma_C^2 & \varsigma_C^3\end{bmatrix}\left(\begin{bmatrix} b_{00} & b_{01} & b_{02} \\ b_{10} & b_{11} & b_{12} \\ b_{20} & b_{21} & b_{22} \\ b_{30} & b_{31} & b_{32}\end{bmatrix}\begin{bmatrix}1 \\ \varsigma_W \\ \varsigma_W^2\end{bmatrix}\right) \end{aligned} \tag{11}$$

The values predicted by means of Eqs. (10) and (11) exhibit a maximum percentage error of 18%, an average percentage error of 4%, and a standard error[36] of 0.1. The model accuracy

Table 6 Regression coefficients to estimate the correction factor k_C according to Eq. (10) or Eq. (11).

Parameter	Sum of squares	Degree of freedom	Mean squares	*F*-statistic	*p*-value
ξ_C	0.00028	1	0.00028	0.94	0.3653
ζ_C	0.00530	2	0.00265	7.81	0.0123
b_C/b_H	0.00456	1	0.00456	15.17	0.0059
Error	0.00210	7	0.00030		
Total	0.01224				

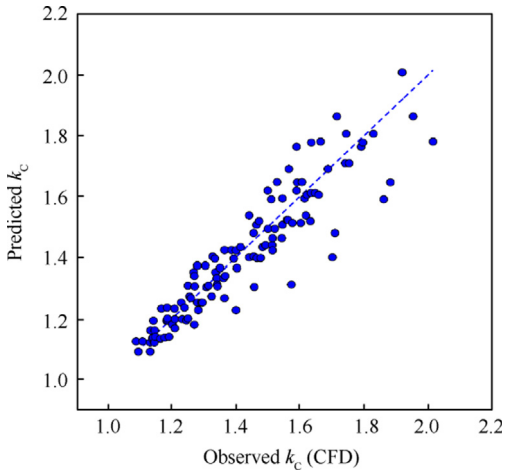

Fig. 15 Correction factor k_C predicted by Eqs. (10)-(11) versus observed values (CFD results) in the full factorial design.

is to be considered acceptable in an engineering perspective, being comparable to the accuracy of other semi-empirical methods commonly used in preliminary aircraft design for the initial sizing and layout evaluation. The values of the correction factors k_C predicted through the proposed method are compared with the observed ones (estimated by means of CFD calculations) in the chart of Fig. 15. The chart shows how the predicted points are quite uniformly distributed around the linear regression. The chart also indicates that the downwash gradient at the horizontal tail is always increased by the presence of a canard since all the values of the correction factors are higher than 1. As the canard lift curve slope increases or the vertical stagger between the canard and the other two lifting surfaces decreases the correction becomes higher. In some cases, the downwash at the tail is almost doubled, that means halving the tail lift contribution (at least in the linear range of angles of attack investigated in this work). By assuming that the tail pitching moment can be simply estimated as the tail lift force times its distance with respect to the aircraft center of gravity, by reducing the lift force the pitching moment due to the tail is decreases with detrimental effects on the aircraft longitudinal stability.

4. Validation case

The prediction formula has been validated against the results from wind tunnel tests on a scaled model of TSA configuration named IRON. Details about the aircraft configuration development and the wind tunnel test campaign have been provided by Nicolosi et al.[12], Corcione et al.[17] and by Cusati et al.[37] The three-view and the main geometrical parameters of the scaled model are shown in Fig. 16. Assuming the superposition principle, the combined downwash of wing and canard on the hori-

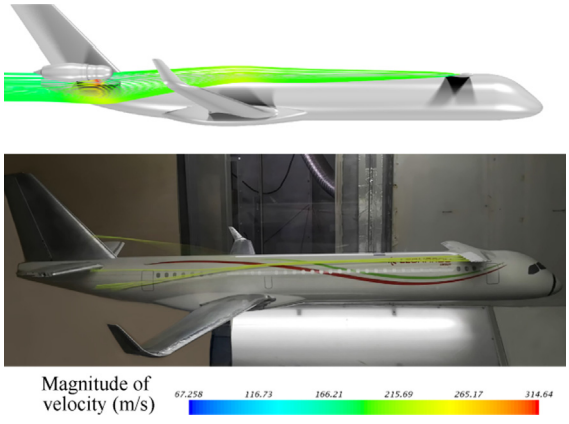

Fig. 17 Streamline visualizations for clean IRON configuration[37] at $\alpha = 0°$. (Top) Viscous CFD simulation, streamlines from right semi-canard trailing edge calculated with STAR-CCM +. (Bottom) Subsonic wind tunnel test, streamlines shown by yellow wool strings attached to the right semi-canard trailing edge.

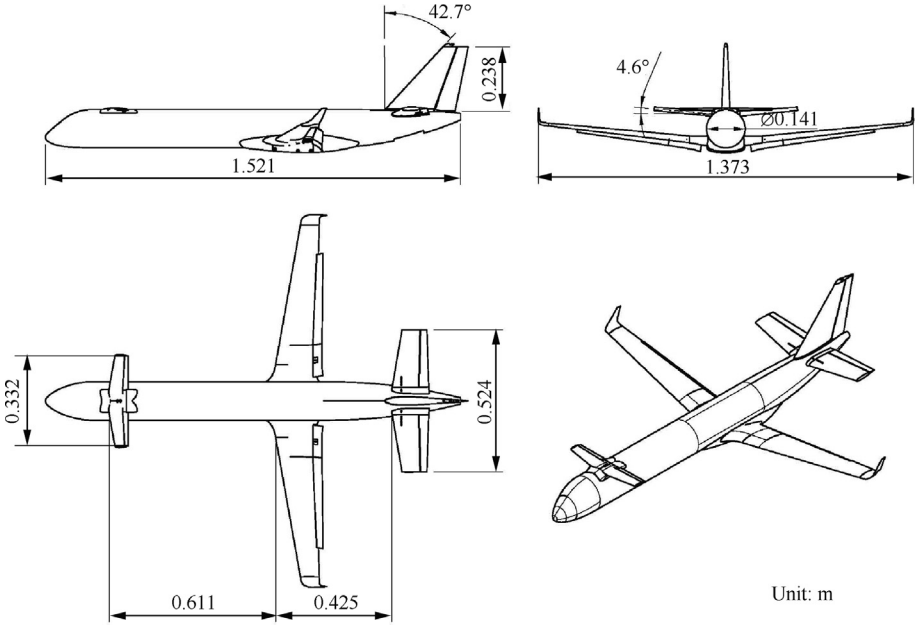

Fig. 16 Scaled aircraft model. Reprinted with permission.[37]

Table 7 Calculated values of correction factor k_C, from CFD numerical results, from wind tunnel test data, and with the proposed Eq. (10) for the IRON three-surface configuration[12,16,17,37]. See also Fig. 17.

ζ_C	ζ_W	b_C/b_H	k_C			Error (%)	
			CFD (inviscid)	Wind Tunnel Tests (WTT)	Proposed Eq. (10)	CFD	WTT
0.04	−0.12	0.6	1.4	1.8	1.6	14	11

zon can be estimated through the comparison of the lift curve slopes of the tail plane with and without the wing and the canard. The tail lift curve slope in presence of the other two lifting surfaces $(C_{L_{\alpha,H}})_{WBHC}$ has been estimated as the difference between the lift curve slope of the Wing-Body-Canard-Horizontal (WBHC) configuration and the Wing-Body (WB). Same consideration holds for the lift curve slope of the isolated tail plane. As suggested by Barlow et al.[31], downwash can be estimated from the experimental data as the ratio of $C_{L_{\alpha,H}}$ between two configurations as reported in Eq. (12).

$$\frac{q_H}{q_\infty}\left(1-\frac{d\varepsilon}{d\alpha}\right)_{WC\ on\ H} = \frac{\overbrace{(C_{L_\alpha})_{WBHC} - (C_{L_\alpha})_{WBHC}}^{(C_{L_{\alpha,H}})_{WBHC}}}{\underbrace{(C_{L_\alpha})_{BH} - (C_{L_\alpha})_B}_{(C_{L_{\alpha,H}})_{BH}}} \tag{12}$$

Streamline visualizations for the clean IRON configuration at $\alpha = 0°$ are shown in Fig. 17. The values of k_C extracted from the numerical and experimental studies on the IRON concept have been compared to the one predicted by the regression formula shown by Eq. (10). These are reported in Table 7, where the percentage errors with respect to both CFD and wind tunnel results, 14% and 11% respectively, confirm the value of the proposed model as a first prediction tool of the average downwash gradient on the tail of three-lifting surface configurations.

5. Conclusions

(1) This work introduces an engineering method to predict the tail downwash gradient of three-lifting-surface aircraft configurations. The prediction approach is based on a correction factor that scales the gradient of a conventional wing-tail combination accounting for the presence of an additional canard surface mounted ahead of the wing. The proposed model is a multivariate polynomial formula obtained as a regression on the results of numerical experiments.

(2) This semi-empirical method has the obvious advantage of being easily applicable to rapidly assess different three-lifting surface layouts in terms of tail downwash.

(3) A natural extension of this research will address the effects of canard on wing design. When the canard span is significantly lower than wingspan, beside the global effect on the tail represented by an average downwash gradient, one must predict also the spanwise downwash induced at the wing. This is important as far as the aerodynamic wing design is concerned when the wing root incidence and the spanwise twist distribution must be selected as a trade-off over different flight conditions.

(4) Yet, the proposed downwash estimation formula is certainly a valuable means able to support the conceptual design of a three-lifting-surface aircraft, in terms of the impact the third lifting surface has on the downwash gradient at the tail and how it affects the aircraft stability in pitch and, consequently, in terms of horizontal tailplane sizing.

Declaration of Competing Interest

The authors declare that they have no known competing financial interests or personal relationships that could have appeared to influence the work reported in this paper.

Acknowledgements

The presented research activity has its roots in a wider investigation that was performed and funded for the development of an innovative high-capacity regional turboprop platform by the IRON project.

The IRON project has received funding from the Clean Sky 2 Joint Undertaking under the European Union's Horimpzon 2020 research and innovation program under Grant Agreement No. 699715. The IRON project is part of Clean Sky 2 REG-GAM 2018 project implemented on the H2020 program under GA 807089The authors are grateful to the partners of the IRON consortium for their contributions and feedback.

References

1. Liebeck R, Page M, Rawdon B. Blended-wing-body subsonic commercial transport. *36th AIAA aerospace sciences meeting and exhibit*; 1998 Jan 12-15; Reno, NV, USA. Reston: AIAA; 1998.
2. Okonkwo P, Smith H. Review of evolving trends in blended wing body aircraft design. *Prog Aerosp Sci* 2016;**82**:1–23.
3. Schiktanz D, Scholz D. Box wing fundamentals - An aircraft design perspective. *German aerospace conference*; 2011 Sep 27-29; Bremen, Germany. 2011.
4. Jemitola P, Fielding J. Box wing aircaft conceptual design. *28th international congress of the aeronautical sciences*; 2012 Sep 23-28; Brisbane, Australia. 2012.
5. Cipolla V, Frediani A, Abu Salem K, et al. Conceptual design of a box-wing aircraft for the air transport of the future. *2018 aviation technology, integration, and operations conference*; 2018 Jun 25-29; Atlanta, Georgia. Reston: AIAA; 2018.
6. Strohmeyer D, Seubert R, Heinze W, et al. Three surface aircraft - A concept for future transport aircraft. *38th aerospace sciences meeting and exhibit*; 2000 Jan 10-13; Reno, NV, USA. Reston: AIAA; 2000.
7. Wichmann G, Strohmeyer D, Streit T. Three-surface aircraft - A concept for future large aircraft. *22nd international congress of aeronautical sciences*; 2000 Aug 27- Sep 1; Harrogate, UK. 2000.

8. Nicolosi F, Corcione S, Della Vecchia P, et al. Aerodynamic design and analysis of an innovative regional turboprop configuration. *31st ICAS conference (International Council of the Aeronautical Sciences*; 2018 Sep 9-14; Belo Horizonte, Brazil. 2018.
9. Goetzendorf-Grabowski T, Antoniewski T. Three surface aircraft (TSA) configuration–flying qualities evaluation. *Aircraft Eng & Aerospace Tech* 2016;**88**(2):277–84.
10. Cacciola S, Riboldi C, Arnoldi M. Three-surface model with redundant longitudinal control: Modeling, trim optimization and control in a preliminary design perspective. *Aerospace* 2021;**8**(5):139.
11. Liersch CM. Was nützt der Canard? Ergebnisse aus dem DLR-Projekt "Dreiflächen-Flugzeug (3FF). *Kolloquium zur Verabschiedung von Dr.-Ing. Günter Redeker*; 2005 Mar 4; Braunschweig, Germany. 2005.
12. Nicolosi F, Corcione S, Ciliberti D, et al. Aerodynamic characteristics of an innovative large turboprop through wind tunnel tests including propulsive effects. *AIAA aviation forum*; 2020 Jun 15-19. Reston: AIAA; 2020.
13. Selberg BP, Rokhsaz K. Aerodynamic tradeoff study of conventional, canard, and trisurface aircraft systems. *J Aircr* 1986;**23**(10):768–74.
14. Ostowari C, Naik D. Experimental study of three-lifting surface configuration. *J Aircr* 1988;**25**(2):106–12.
15. Patek Z, Smrcek L. Aerodynamic characteristics of multi-surface aircraft configurations. *Aircr Des* 1999;**2**(4):191–206.
16. Nicolosi F, Corcione S, Trifari V, et al. Design and optimization of a large turboprop aircraft. *Aerospace* 2021;**8**(5):132.
17. Corcione S, Nicolosi F, Della Vecchia P, et al. High lift aerodynamic characteristics of a three lifting surfaces turboprop aircraft. *AIAA aviation 2019 forum*; 2019 Jun 17-21; Dallas, Texas. Reston: AIAA; 2019.
18. Ruiz-Calavera LP, Martínez-Val R, Gómez-Blanco R. Minimum induced drag of a three-surface ultra high capacity aircraft. *Proc Inst Mech Eng Part G J Aerosp Eng* 1995;**209**(3):195–201.
19. Owens DB, Perkins JN. Stability and control of a three-surface, forward-swept wing configuration. *J Aircr* 1996;**33**(6):1206–8.
20. Roskam J. *Airplane flight dynamics and automatic flight controls*. 3rd ed. Kansas: Lawrence; 2003.
21. Silverstain A, Katzoff S, Bullivant S, et al. Downwash and wake behind plain and flapped wings. Washington, D.C.: Laboratories Langley Field; 1939. Report No.: NACA-TR-651.
22. Silverstein A, Katzoff S. Design charts for predicting downwash angles and wake characteristics behind plain and flapped wings. Washington, D.C.: Laboratories Langley Field; 1939. Report No.: NACA-TR-648.
23. Finck RD. USAF (United States air force) stability and control DATCOM (data compendium). St. Louis (USA): McDonnel Douglas Astronautics Company; 1977.
24. Slingerland R. Prediction of a tail downwash, ground effect and minimum unstick speed of jet transport aircraft [dissertation]. Delft (Netherlands): Technical University of Delft; 2005.
25. Philips JD. Downwash in the plane of symmetry of an elliptically loaded wing. Moffett Field(CA): NASA Ames Research Center; 1985. Report No: NASA Technical Paper 2414.
26. Philips JD. Approximate neutral point of a subsonic canard aircraft. Moffett Field(CA): NASA Ames Research Center; 1985. Report No.: NASA Technical Memorandum 86694.
27. Rasmussen ML. The effect of a canard surface on the total lift of an unswept wing in subsonic flow [dissertation]. Oregon (USA): Oregon State University; 1959.
28. Levy DW. Prediction of average downwash gradient for canard configurations. *30th aerospace sciences meeting and exhibit*; 1992 Jan 6-9; Reno, NV, USA. Reston: AIAA; 1992.
29. De Marco A, Di Stasio M, Della Vecchia P, et al. Automatic modeling of aircraft external geometries for preliminary design workflows. *Aerosp Sci Technol* 2020;**98:** 105667.
30. Simcenter[Internet]. Munich: Siemens Germany [updated 2022 Mar 17, cited 2022 Mar 17]. Available from: https://www.plm.automation.siemens.com/global/it/products/simcenter/.
31. Barlow JB, Rae WH, Pope A. *Low-speed wind tunnel testing*. 3rd ed. Hoboken: John Wiley & Sons, Inc.; 1999.
32. Anthony J. *Design of experiments for engineers and scientists*. 2nd ed. Amsterdam: Elsevier Ltd; 2014. p. 63–85.
33. Jansen Q. *Relaxed static stability performance assessment on conventional and unconventional aircraft configurations[dissertation]*. Delft (Netherlands): Technical University of Delft; 2015.
34. MATLAB Statistics and Machine Learning Toolbox[Internet]. Natick, MA: The MathWork, Inc.; 2021. Available from: http://ww2.mathworks.com.
35. Montgomery DC. *Design and analysis of experiments*. 8th ed. Hoboken: John Wiley & Sons, Inc.; 2017.
36. Andrade C. Understanding the difference between standard deviation and standard error of the mean, and knowing when to use which. *Indian J Psychol Med* 2020;**42**(4):409–10.
37. Cusati V, Corcione S, Ciliberti D, et al. Design evolution and wind tunnel tests of a three-lifting surface regional transport aircraft. *Aerospace* 2022;**9**(3):133.